Eur. Phys. J. A (2023) 59:178
https://doi.org/10.1140/epja/s10050-023-01095-4

THE EUROPEAN PHYSICAL JOURNAL A

Regular Article - Theoretical Physics

TALYS calculations of prompt fission observables and independent fission product yields for the neutron-induced fission of ^{235}U

Kazuki Fujio[1,a], **Ali Al-Adili**[2], **Fredrik Nordström**[2], **Jean-François Lemaître**[3], **Shin Okumura**[4], **Satoshi Chiba**[5,6], **Arjan Koning**[4]

[1] Nuclear Engineering Course, Department of Transdisciplinary Science and Technology, School of Environment and Society, Tokyo Institute of Technology, 2-12-1 Ookayama, Meguro, Tokyo 152-8550, Japan
[2] Department of Physics and Astronomy, Uppsala University, 751 20, Uppsala, Sweden
[3] CEA-DAM Île-de-France, Bruyères-le-Châtel, 91297 Arpajon Cedex, France
[4] NAPC-Nuclear Data Section, International Atomic Energy Agency, Vienna International Centre, 1400 Vienna, Austria
[5] NAT Research Center, NAT Corporation, 3129-45 Hibara, Muramatsu, Tokai-mura, Naka-gun, Ibaraki 319-1112, Japan
[6] Tokyo Institute of Technology, 2-12-1 Ookayama, Meguro, Tokyo 152-8550, Japan

Received: 14 April 2023 / Accepted: 24 July 2023 / Published online: 3 August 2023

Communicated by Cedric Simenel

Abstract The TALYS nuclear reaction code's Hauser-Feshbach statistical decay model has been adapted in order to calculate prompt fission neutron and γ-ray observables by iterating over deexciting fission fragments. Several fission fragment generators such as GEF, HF^{3}D, and SPY were employed to provide TALYS with databases. These databases contain standardized tables with fission fragment yields, mean excitation energies and their widths, and average total kinetic energy, as a function of charge and mass number of primary fission fragments. The resulting calculations, including prompt particle multiplicities, spectra, average energies, and independent fission product yields, were compared with experimental and evaluated data. This work first outlines the new methodology implemented in TALYS and examines the effects of three important parameters on the final evaporation data. Furthermore, the neutron-induced fission of ^{235}U is investigated in detail as a function of incident energy. The results from TALYS, with input from GEF and HF^{3}D, were compared with available experimental data and the results of the stand-alone GEF code. The proposed methodology contributes to an improved capability to model the fission process.

1 Introduction

Prompt particle emission from primary fission fragments during the nuclear fission process generates various correlated prompt fission quantities. These include independent fission product yields, prompt fission neutron multiplicities $\bar{\nu}_n$, prompt fission neutron spectra (PFNS), prompt fission γ-ray multiplicities $\bar{\nu}_\gamma$, prompt fission γ-ray spectra (PFGS) and isomeric yield ratios. The characteristics of these prompt fission quantities contain valuable information for a detailed understanding of fission physics and are beneficial for many nuclear applications; e.g., the evaluation of delayed neutron yields for reactor safety [1], design of a transmutation systems for minor actinides in nuclear waste management [2], producing radioisotopes for diagnosis and therapy [3], and studying nuclear astrophysics, especially during the fission cycle in the r-process.

However, comprehensive modeling of these observables for different fissioning systems at various excitation energies remains challenging. Moreover, the estimation of accurate fission observables required for the aforementioned applications still relies on empirical models. For instance, Wahl systematics for fission yields [4–6], and Madland-England model [7] for isomeric ratios have been used in ENDF/B-VIII [8] and JENDL-4.0 [9] evaluations. The Los Alamos (Madland-Nix) model for PFNS [10] is based on physical considerations; however, it takes into account only one fragmentation (the so-called most probable fragmentation).

During the fission process, the compound nucleus undergoes deformation, therefore, may approach the scission point. In binary fission, the nucleus splits into two complementary fission fragments. Typically, this process may lead to several hundred different fission fragment pairs. After the mass split, the Coulomb repulsion between the nascent fragments accelerates them, back-to-back. The summation of the excitation energy of the compound nucleus and the Q-value of the reac-

[a] e-mail: fujio.k.aa@m.titech.ac.jp (corresponding author)

tion is divided between the total kinetic energy (TKE) and the total excitation energy (TXE). When the fragments reach their full acceleration, the highly excited fragments deexcite by emitting prompt fission neutrons and prompt fission γ-rays until they reach their metastables or ground states. Then the fission products undergo β^- decay. β^- decay takes place in neutron-rich independent fission products. The delayed neutrons and delayed γ-rays are emitted from the independent fission products to become the final stable or long-lived cumulative fission products.

Since the fission process consists of several different physical phenomena, the stages are described by different physics. The current modeling for the prompt fission observables often does not consider correlations among the independent fission product yield and the other prompt fission observables, which partly causes inconsistency in the model calculations [11]. Therefore, more recently, studies are also being conducted to evaluate prompt fission observables consistently.

Several computer programs have been developed to simulate the particle emission based on the sequential emission from the excited fission fragments with or without applying the Hauser-Feshbach statistical decay theory. These codes are either by Monte Carlo samplings, such as CGMF [12,13], FREYA [14,15], FIFRELIN [16–18], and GEF [19], or by deterministic approaches, such as the Point-by-Point model (PbP) [20], the Deterministic Sequential Emission model (DSE) [21], and HF^{3}D [22–24].

In this study, we propose the use of a common, consistent, well-documented, and transparent nuclear deexcitation code to probe biases and systematic errors in the initial assumptions in fission physics. These systematic errors can be compensated by fine-tuning parameters during the deexcitation stage. We employ existing fission fragment generators to yield pre-neutron emission fission fragment mass and energy yield distributions, including both microscopic models [25] and phenomenological models [19,22,23]. The nuclear reaction model code TALYS [26] calculates the evaporation of neutrons and γ-rays from the excited fission fragment to obtain prompt fission observables. In the Hauser-Feshbach statistical decay calculation, TALYS adopts deterministic techniques similar to the HF^{3}D model [22,23], while so far the calculation is limited to the first-chance fission only, in which no neutron is evaporated prior to fission.

We examine the detailed calculation of the neutron-induced fission on ^{235}U and show the calculated neutron and γ-ray multiplicities, PFNS, PFGS, and independent fission product yields, which are compared with the available experimental and evaluated data.

2 Fission models in TALYS

The TALYS code (version: 1.96) includes several modules for calculating fission observables. The first implementation of mass yields in TALYS was based on a revised version of the multi-modal random neck-rupture model (MM-RNRM). The original model was developed by Brosa [27] to calculate the properties of fission fragments at zero temperature. The temperature is added to the model calculation of the potential energy landscape of the nucleus [28]. A search for the fission channels in deformation space yields the superlong (SL), standard I (ST I), and standard II (ST II) fission barriers and pre-scission shapes as a function of temperature. The obtained temperature-dependent fission barrier and pre-scission shape parameters serve as an input option for the fragment mass distribution computations in TALYS. However, this model fails to agree with most experimental fission yields [29]. Another approach to enhance the pre-neutron mass distributions was to combine the GEF code with TALYS through direct code translation to Fortran. However, this method locks the code version and does not facilitate a smooth transition to an updated fission code version. It can also result in large discrepancies compared to recent versions of GEF [30].

A third approach was recently implemented [31,32] and makes use of phenomenological and empirical codes, such as GEF [19,30], HF^{3}D [22,23], and SPY [25,33], as fission fragment generators to create a fission fragment database for TALYS. Employing these databases one can facilitate comprehensive model comparisons that address systematic errors and model defects. Figure 1 shows the workflow of the intended approach. The starting point involves the initial conditions defined by the fission fragment yield $Y_{\rm ff}(Z, A)$ for each fragment charge Z and mass number A, the mean excitation energy $\bar{E}_x$ of its Gaussian distribution, the width σ_{E_x} of the excitation energy distribution, and average total kinetic energy ($\overline{\rm TKE}$) for fragment pair. TALYS uses these databases to calculate evaporation data, e.g., neutron and γ-ray emissions sequentially until both fragments are relaxed and reach their ground states. In this methodology, one may iterate the calculations to tweak parameters and perform sensitivity studies to reveal compensating trends and other correlated effects [34,35].

2.1 Generating fission fragment distribution database

This section describes two models of fission fragment generators used to produce fission fragment databases as input to TALYS. The first model, HF^{3}D (Hauser-Feshbach Fission Fragment Decay), which is a statistical decay code [22,23], has been developed to study prompt neutron and γ-ray observables from the neutron-induced fission of ^{235}U, ^{238}U, and ^{239}Pu by the Hauser-Feshbach statistical decay code,

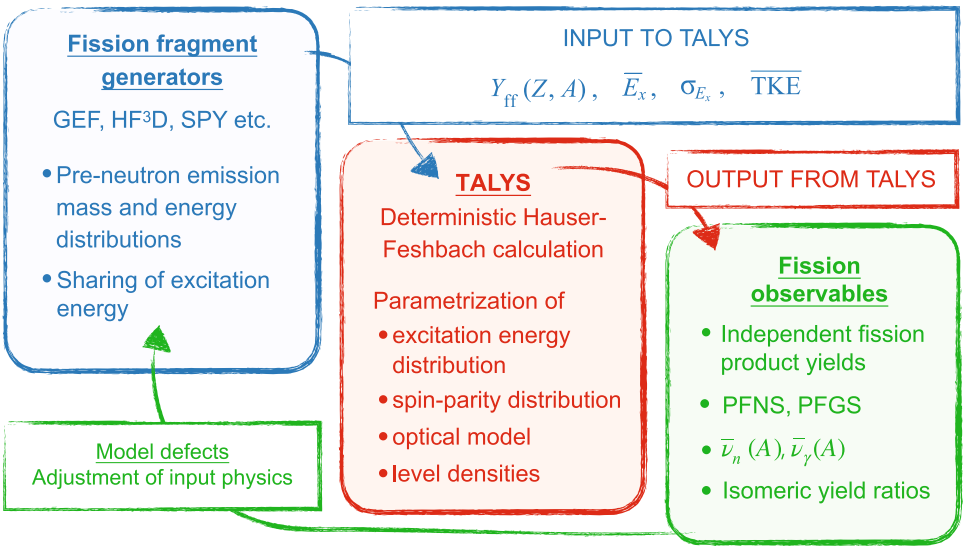

Fig. 1 The proposed workflow, where various fission models are used to create pre-neutron emission databases for TALYS. The necessary inputs to TALYS are fission fragment yields $Y_{\rm ff}(Z, A)$, the mean excitation energy $\bar{E}_x$, its width σ_{E_x}, and average total kinetic energy ($\overline{\rm TKE}$). The output from the Hauser-Feshbach formalism of TALYS yields deexcitation data that can be compared with experimental data and with results from other stand-alone model codes. The methodology facilitates comprehensive model comparison addressing systematic errors and model defects

BeoH, with the deterministic approach so that it can calculate contributions including fission fragments having very low yield and also to ensure that isomeric production comes from a proper decay scheme including discrete level information. In the HF^{3}D model, the fission fragment distribution is generated by fitting the experimentally available $Y_{\rm ff}(A)$, $\overline{\rm TKE}(A)$ data and distributing excitation energy between the complement fission fragments based on a ratio of nuclear temperatures, the anisothermal model parameter R_T [36]. The generated ($Y_{\rm ff}(Z, A)$, $\bar{E}_x$, σ_{E_x}, $\overline{\rm TKE}$) are stored in the TALYS fission fragment database in tabulated format.

The second model, GEF [37], is a Monte Carlo-based phenomenological fission model that generates both pre-neutron emission quantities as well as deexcitation data, albeit by employing a simple evaporation scheme. In this work, GEF (version: 2021/1.2) was employed to produce the mass and charge yields of primary fission fragments and corresponding energies [30]. The Monte Carlo sampling was based on 1 million fission events for every reaction. The list-mode data feature was activated to allow for an event-by-event output of each fission simulation. In total, data files from 737 fissioning nuclei were calculated, ranging from $_{76}$Os to $_{115}$Mc, at excitation energies ranging from 0 to 20 MeV. The generated ($Y_{\rm ff}(Z, A)$, $\bar{E}_x$, σ_{E_x}, $\overline{\rm TKE}$) were stored in the TALYS fission fragment database in a tabulated format. The data were modified to include only first-chance fission. In the future, TALYS will be responsible for assigning the multi-chance fission probability, thus allowing for interpolation between first-chance fission files.

3 Deterministic approach to the fission fragment deexcitation

3.1 Generating the initial distributions

TALYS calculates fission fragment deexcitation by integrating the Hauser-Feshbach statistical decay calculation over the distribution for all fission fragments, instead of Monte Carlo sampling. The main advantage of the deterministic treatment is that this can take account into the small probability of fission events. A technique for this is explained in Refs. [22–24].

Figure 2 shows a schematic view of the multiple neutron and γ-ray emission process from an excited fission fragment (Z, A). The initial fragment (Z, A) is in the continuum excited state and it decays to either the continuum or discrete states of $(Z, A-1)$ by emitting a neutron and either the continuum or discrete states of (Z, A) by emitting γ-rays. This sequential process continues until each state reaches the ground or isomeric state.

To calculate such a deexcitation process, it requires the primary fission fragments' quantities. TALYS reads such initial distributions from the fission fragment databases described above and builds an excitation energy distribution $G(E_x)$ and a spin-parity distribution $R(J, \pi, E_x)$. The initial population $P_{0,Z,A}$ of a given fission fragment is expressed as follows:

$$P_{0,Z,A}(J, \pi, E_x) = R(J, \pi, E_x)G(E_x). \quad (1)$$

TALYS assumes a Gaussian fragment excitation energy distribution with the mean excitation energy $\bar{E}_x$ and the width σ_{E_x},

$$G(E_x) = \frac{1}{\sqrt{2\pi}\sigma_{E_x}} \exp\left\{-\frac{(E_x - \bar{E}_x)^2}{2\sigma_{E_x}^2}\right\}. \quad (2)$$

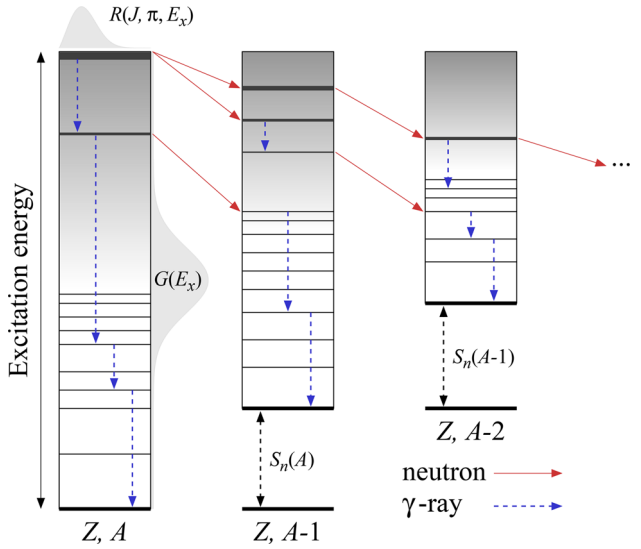

Fig. 2 Schematic view of the multiple neutron and γ-ray emission process from a fission fragment (Z, A). The vertical axis shows the excitation energy and S_n is the neutron separation energy. The solid arrows represent neutron emission and the dashed vertical arrows represent γ-ray emission

The angular momentum generation remains a challenge for contemporary fission modeling [38–42]. TALYS adopts the spin-parity distribution $R(J, \pi, E_x)$ by following the functional dependency of the level density formula [43]. Since the parity distribution is 1/2, the spin-parity distribution $R(J, \pi, E_x)$ is assumed to be expressed as

$$R(J, \pi, E_x) = \frac{1}{2} \cdot \frac{2J+1}{2f^2\sigma^2(E_x)} \exp\left\{-\frac{(J+1/2)^2}{2f^2\sigma^2(E_x)}\right\}. \quad (3)$$

A scaling factor f^2 is introduced in order to assure a reasonable agreement with experimental data. This new scaling parameter controls the distribution of angular momenta for primary fission fragments.

Another important parameter is the spin cut-off parameter $\sigma^2(E_x)$ entering a level density model [44,45], defined as

$$\sigma^2(E_x) = 0.01389 \frac{A^{5/3}}{\tilde{a}} \sqrt{a(E_x - \Delta)}, \quad (4)$$

where Δ is the pairing energy correction, $\tilde{a}$ is the asymptotic level density parameter, and a is the level density parameter. TALYS uses another scaling factor, f_s, which represents a global adjustment factor of the nuclear spin cut-off parameter, applicable for the level density model. This parameter is multiplied to $\sigma^2(E_x)$ and affects all independent fission products which are populated by the emission of prompt neutrons. The distributions $G(E_x)$ and $R(J, \pi, E_x)$ should satisfy the normalization condition, i.e., $\int G(E_x)dE_x = 1$ and $\sum_{J\pi} R(J, \pi, E_x) = 1$.

The other ingredients in the Hauser-Feshbach model calculations include the optical model potentials for neutron and charged particles, the level density parameters, the γ-ray strength function, and the discrete level properties for all residual nuclei. For this study, we used the Koning-Delaroche global optical potential [46] for neutrons, a composite level density formula (Gilbert and Cameron model [47]) using the level density parameters and systematics from Ref. [48], IAEA-CRP SMLO 2019 tables and IAEA GSF CRP 2018 for E1 and M1 γ-ray strength functions [49–51], and the discrete level data from RIPL-3 [52].

3.2 Calculated prompt fission observables

The statistical Hauser-Feshbach calculation is performed from the initial condition (J, π, E_x) of a fission fragment (Z, A) while the results for the emitted neutrons and γ-rays are $\nu_n(Z, A, J, \pi, E_x)$ and $\nu_\gamma(Z, A, J, \pi, E_x)$. These results are then weighted using the initial fission yields to calculate the final observables.

The prompt fission neutron multiplicity $\bar{\nu}_n(Z, A)$ of a given fission fragment is calculated by adding the fission neutron production resulting from the initial population $P_{0,Z,A}(J, \pi, E_x)$,

$$\bar{\nu}_n(Z, A) = \int\int \sum_{J,\pi} \nu_n(Z, A, J, \pi, E_x) \times \mathrm{PFNS}_{(\mathrm{CMS})(Z,A,J,\pi)}(\epsilon) P_{0,Z,A}(J, \pi, E_x) d\epsilon dE_x, \quad (5)$$

where $\nu_n(Z, A, J, \pi, E_x)$ is the neutron multiplicity and $\mathrm{PFNS}_{(\mathrm{CMS})(Z,A,J,\pi)}(\epsilon)$ is the neutron kinetic energy spectrum in center-of-mass system (CMS). The $\mathrm{PFNS}_{(\mathrm{CMS})(Z,A)}(\epsilon)$ produced by the fragment (Z, A) is given by

$$\mathrm{PFNS}_{(\mathrm{CMS})(Z,A)}(\epsilon) = \frac{1}{\bar{\nu}_n(Z, A)} \int \sum_{J,\pi} \nu_n(Z, A, J, \pi, E_x) \times \mathrm{PFNS}_{(\mathrm{CMS})(Z,A,J,\pi)}(\epsilon) P_{0,Z,A}(J, \pi, E_x) dE_x. \quad (6)$$

The fission neutron spectrum of a fragment in the laboratory frame, $\mathrm{PFNS}_{(\mathrm{LAB})(Z,A)}(E)$, is converted from the center-of-mass system by Feather's formula [53–55]:

$$\mathrm{PFNS}_{(\mathrm{LAB})}(E) = \int_{(\sqrt{E}-\sqrt{E_f})^2}^{(\sqrt{E}+\sqrt{E_f})^2} \frac{\mathrm{PFNS}_{(\mathrm{CMS})}(\epsilon)}{4\sqrt{E_f}\sqrt{\epsilon}} d\epsilon, \quad (7)$$

where E_f is the kinetic energy per nucleon of the fission fragment. The PFNS is usually plotted as ratio to a Maxwellian spectrum:

$$\phi_M(E) = \frac{2}{\sqrt{\pi T_M^3}} \sqrt{E} \exp\left(-\frac{E}{T_M}\right). \quad (8)$$

In this work, we adopted $T_M = 1.32$ MeV for comparison with experimental and evaluated data.

The γ-ray observables can be obtained in a similar way to the neutron observables. The prompt fission γ-ray multiplicity $\bar{\nu}_\gamma(Z, A)$ is calculated by using the initial population and

the γ-ray spectrum $\mathrm{PFGS}_{(Z,A,J,\pi)}(\epsilon)$ in the center-of-mass system:

$$\bar{\nu}_\gamma(Z,A) = \int\int \sum_{J,\pi} \nu_\gamma(Z,A,J,\pi,E_x) \times \mathrm{PFGS}_{(Z,A,J,\pi)}(\epsilon) P_{0,Z,A}(J,\pi,E_x) d\epsilon dE_x. \quad (9)$$

The $\mathrm{PFGS}_{(Z,A)}(E)$ produced by the fragment (Z, A) is given by

$$\mathrm{PFGS}_{(Z,A)}(\epsilon) = \int \sum_{J,\pi} \nu_\gamma(Z,A,J,\pi,E_x) \times \mathrm{PFGS}_{(Z,A,J,\pi)}(\epsilon) P_{0,Z,A}(J,\pi,E_x) dE_x. \quad (10)$$

Due to prompt neutron emission, the mirror symmetry seen in the primary fission fragment yield is broken and characteristic peaks appear. The independent fission product yield $Y(Z, A)$ is deduced from the primary fission fragment yields $Y_{\mathrm{ff}}(Z, A)$:

$$Y(Z,A) = \sum_{\nu} P_{Z,A+\nu}(\nu) Y_{\mathrm{ff}}(Z, A+\nu), \quad (11)$$

where $P_{Z,A}(\nu)$ is the probability to emit ν neutrons by the primary fragment (Z, A).

4 Results and discussion

4.1 Sensitivity of fission observables on input parameters

We identified several key input parameters essential for controlling the statistical decay calculation of fission fragments. To evaluate the observables from the fission fragment deexcitation, a sensitivity study was performed on the spin-parity distribution and the number of continuum states. The scaling factor f^2 in Eq. (3) modulates the angular momentum distribution. The other scaling factor adjusts the spin cut-off parameter, $\sigma^2(E_x)$, by the multiplication factor f_s. The energy width of discretized continuum state Δ_{bins} is given by

$$\Delta_{\mathrm{bins}}(Z,A) = (E_x^{\mathrm{max}} - E_x^{\mathrm{level}})/N, \quad (12)$$

where N is the number of continuum states, E_x^{max} is the maximum excitation energy, and E_x^{level} is the excitation energy of the last discrete level. In TALYS, N varies in response to the number of nucleons emitted. If the number of emitted nucleons is less than 4, the value of N remains the same as the input value. However, if the number of emitted nucleons is less than 8, the revised number of continuum states denoted as N' can be: $N' = (1 - 0.1(x - 4)) \times N$, where x is the number of emitted nucleons. If the number of emitted nucleons is greater than 8, the value of N' is reduced to half of the initial value of N.

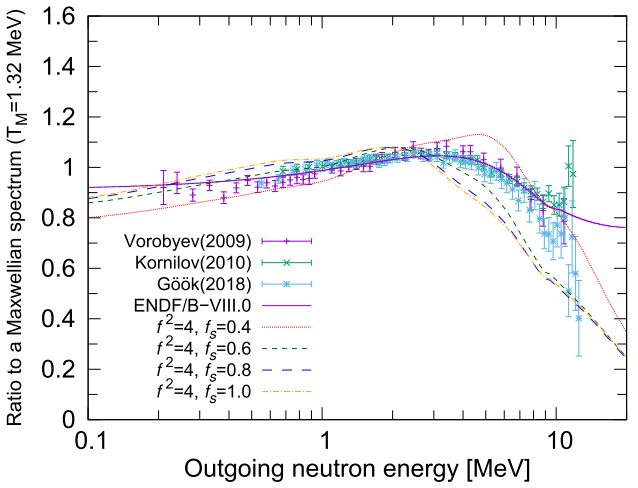

Fig. 3 Sensitivity of spin cut-off parameters on $\mathrm{PFNS}_{(\mathrm{LAB})}$ as ratio to a Maxwellian spectrum at $T_M = 1.32$ MeV with $N = 300$. The reaction is $^{235}\mathrm{U}(\mathrm{n_{th}},\mathrm{f})$, and the input data is obtained from $\mathrm{HF}^3\mathrm{D}$ model

4.1.1 Sensitivity on spin cut-off parameters

In our previous investigation [22], the $\mathrm{HF}^3\mathrm{D}$ model indicated that $f = 2.5$ was necessary to reproduce the neutron observables in the neutron-induced fission of ^{235}U up to 5 MeV incident energy. We have chosen to set f^2 to a range of 4–6, based on rough estimates from the same study [22]. Additionally, another recent study [56] has suggested that setting f_s within the range of 0.4–0.5 is optimal for reproducing isomeric yield ratios observed in experiments involving neutron capture and other reactions.

We conducted a sensitivity analysis by varying the f^2 parameter between 3 and 6 (changing in unit steps), and the f_s parameter between 0.4 and 1.0 (changing by 0.2 in step size). The input for the TALYS calculation was based on $(Y_{\mathrm{ff}}(Z,A), \bar{E}_x, \sigma_{E_x}, \overline{\mathrm{TKE}})$ obtained from $\mathrm{HF}^3\mathrm{D}$. Table 1 presents a summary of the calculated values for $\bar{\nu}_\gamma$, $\bar{\nu}_n$, $\langle\epsilon_\gamma\rangle$, and $\langle\epsilon_n\rangle$. Results obtained with $f^2 = 4$ yield better $\bar{\nu}_n$ values, but smaller $\bar{\nu}_\gamma$ compared to those obtained with $f^2 = 5, 6$. The results indicate a clear trend in which $\langle\epsilon_\gamma\rangle$ decreases with increasing values of f^2 and f_s, respectively. $\langle\epsilon_n\rangle$ also decreases as f_s increases. Figure 3 shows the calculated $\mathrm{PFNS}_{(\mathrm{LAB})}$ as ratio to a Maxwellian spectrum with $f^2 = 4$ that gives good $\bar{\nu}_n$. f_s value has a significant impact on both the peak position and shape of the $\mathrm{PFNS}_{(\mathrm{LAB})}$ above 2 MeV. Our priority is to accurately reproduce the neutron observables, particularly $\bar{\nu}_n$. Therefore, the optimal spin cut-off parameters are $f^2 = 4$ and $f_s = 0.4$ (see Table 1).

4.1.2 Sensitivity on the number of continuum states

A sensitivity analysis was performed to study the role of the number of continuum states, N. The $\mathrm{HF}^3\mathrm{D}$ model employs

Table 1 Sensitivity of prompt neutron and γ-ray multiplicities ($\bar{\nu}_n$ and $\bar{\nu}_\gamma$, respectively) and average energies ($\langle\epsilon_n\rangle$ and $\langle\epsilon_\gamma\rangle$, respectively) to changes in the spin cut-off parameters for the ^{235}U(n$_{th}$,f) reaction. $\langle\epsilon_n\rangle$ is given in the laboratory frame (LAB), while $\langle\epsilon_\gamma\rangle$ is given in the center-of-mass system (CMS)

TALYS (HF^{3}D)						
# of N	f^2	f_s	$\bar{\nu}_\gamma$	$\bar{\nu}_n$	$\langle\epsilon_\gamma\rangle$ (MeV)	$\langle\epsilon_n\rangle$ (MeV)
300	3	0.4	5.06	2.49	0.869	2.049
	3	0.6	5.76	2.47	0.818	1.945
	3	0.8	6.21	2.45	0.786	1.915
	3	1.0	6.50	2.44	0.764	1.907
	4	0.4	6.05	2.41	0.772	2.079
	4	0.6	6.92	2.40	0.728	1.941
	4	0.8	7.48	2.39	0.699	1.899
	4	1.0	7.85	2.38	0.677	1.887
	5	0.4	6.85	2.35	0.714	2.107
	5	0.6	7.90	2.34	0.675	1.938
	5	0.8	8.55	2.33	0.646	1.886
	5	1.0	8.96	2.33	0.625	1.869
	6	0.4	7.45	2.30	0.681	2.132
	6	0.6	8.66	2.29	0.646	1.935
	6	0.8	9.36	2.29	0.617	1.876
	6	1.0	9.85	2.29	0.593	1.855
ENDF-B/VIII.0 [8]			8.58	2.41	0.85	2.00
JEFF-3.3 [57]			8.74	2.41	0.81	

Table 2 Sensitivity of prompt neutron and γ-ray multiplicities ($\bar{\nu}_n$ and $\bar{\nu}_\gamma$, respectively) and average energies ($\langle\epsilon_n\rangle$ and $\langle\epsilon_\gamma\rangle$, respectively) to changes in N for the ^{235}U(n$_{th}$,f) reaction. $\langle\epsilon_n\rangle$ is given in the laboratory frame (LAB), while $\langle\epsilon_\gamma\rangle$ is given in the center-of-mass system (CMS)

TALYS (HF^{3}D)						
# of N	f^2	f_s	$\bar{\nu}_\gamma$	$\bar{\nu}_n$	$\langle\epsilon_\gamma\rangle$ (MeV)	$\langle\epsilon_n\rangle$ (MeV)
50	4	0.4	3.46	2.49	1.192	1.990
100	4	0.4	4.87	2.43	0.923	2.045
200	4	0.4	5.78	2.41	0.804	2.072
300	4	0.4	6.05	2.41	0.772	2.079
ENDF-B/VIII.0 [8]			8.58	2.41	0.85	2.00
JEFF-3.3 [57]			8.74	2.41	0.81	

a constant Δ_{bins} size of 100 keV for both the primary fission fragment and the decaying nucleus, while TALYS partitioned the excitation energy into the specified number of N. To ensure a maximum Δ_{bins} size of 500 keV, we set the N range to be between 50 and 300. Regarding γ-ray observables, both $\bar{\nu}_\gamma$ and the prompt fission γ-ray spectrum (PFGS) multiplied by $\bar{\nu}_\gamma$ exhibit sensitivity to N. As seen in Table 2, the higher N value leads to more emitted γ-rays. A broader spin distribution also increases the average spin of the fission fragment. Fission fragments with high angular momenta are unable to reach low-excitation levels directly since the γ-ray transition is generally governed by dipole transitions. Therefore, larger values of initial spins lead to an increase in the number of emitted γ-rays. This stands in contrast to neutron emissions, highlighting a significant difference between the two types of emissions. The $\bar{\nu}_\gamma$ also becomes large as N increases because the number of continuum states increases as well. TALYS sequentially gives the same number of bins to the residual nucleus as the input, therefore, the size of bins becomes smaller as neutrons are emitted. Figure 4a shows $\bar{\nu}_\gamma(A)$, and (b) shows PFGS with different number of N. It is suggested that the prominent peak below 0.2 MeV in PFGS is mainly caused by the number of continuum states effect. We have verified that the impact of the bins parameter on neutron observables is negligible, and thus we select $N = 300$ for improved consistency with experimental and evaluated data. Regarding independent fission product yield, we have confirmed that the effects of these parameters are sufficiently insignificant.

Consequently, we have identified the input parameter set, consisting of $f^2 = 4$, $f_s = 0.4$, and $N = 300$, as the optimal selection for obtaining accurate prompt neutron multiplicity and better γ-ray observables at thermal energy.

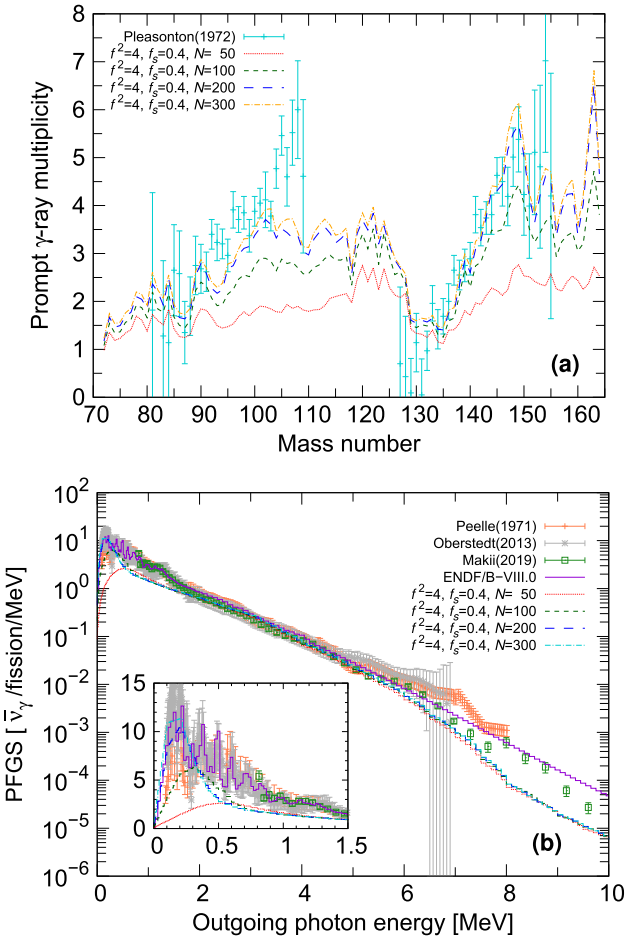

Fig. 4 Sensitivity on N of fragments after the first neutron emission to **a** the mass-dependent γ-ray multiplicity and **b** PFGS multiplied by the γ-ray multiplicity. Both calculations are the ^{235}U(n$_{th}$,f) reaction, and the input data is obtained from HF^{3}D model. The enlarged view of the lower energy region is displayed in the inset of the **b**

4.2 Application of the present method to neutron-induced fission of ^{235}U

In this section, we compare the TALYS calculation of fission observables with experimental and evaluated data of ^{235}U(n,f) in the incident energy range from thermal up to 5 MeV. The calculations were performed for two sets of input data, namely:

1. TALYS Hauser-Feshbach statistical decay employing the fission fragment distributions from HF^{3}D (denoted in the following as TALYS(HF^{3}D)),
2. TALYS Hauser-Feshbach statistical decay utilizing the fission fragment distributions from GEF (denoted in the following as TALYS(GEF).

The results of the stand-alone GEF code are also plotted, they being denoted as GEF. The comparison between TALYS(GEF) and stand-alone GEF highlights important differences in the deexcitation procedure, and might shed light on valuable model discrepancies, given that the very same input pre-neutron data was employed.

4.2.1 *Prompt neutron observables*

Figure 5a shows the $\bar{\nu}_n(A)$ at thermal neutron energy. The $\bar{\nu}_n(A)$ calculated by TALYS(GEF), TALYS(HF^{3}D), and GEF all show the saw-tooth shape that is consistent with experimental data. The TALYS(HF^{3}D) agrees fairly well with the experimental data, around the most probable masses. However, for far asymmetric mass splits, larger discrepancies are observed. In case of TALYS(GEF) and GEF however, a clear overestimation can be seen in $\bar{\nu}_n(A)$ for the heavy fragments and underestimates the $\bar{\nu}_n(A)$ for the light mass region, compared both with the TALYS(HF^{3}D) and the literature data. Around double magicity, $Z = 50$ and $N = 82$, the $\bar{\nu}_n(A)$ exhibits a pronounced minimum. Recent experimental findings indicate a striking shift towards lighter masses [58].

Table 3 shows a summary of the calculated $\bar{\nu}_n$, $\bar{\nu}_\gamma$, average energy of neutrons and γ-rays, denoted as $\langle\epsilon_n\rangle$ and $\langle\epsilon_\gamma\rangle$, respectively, obtained from TALYS(GEF), TALYS(HF^{3}D), and GEF, along with experimental and evaluated data for comparison. The $\bar{\nu}_n$ from TALYS(GEF) is lower than that from GEF because $\bar{\nu}_n(A)$ is lower over a wide mass range. Comparing TALYS(GEF) and GEF with experimental data, the $\bar{\nu}_n(A)$ underestimates in the light fragment and overestimates in the heavy fragment. These deviations cancel each other, therefore, both of $\bar{\nu}_n$ are in good agreement with the evaluated data. For $\langle\epsilon_n\rangle$, both TALYS results agree with the evaluated value.

$\bar{\nu}_n(A)$ of ^{235}U(n,f) at the incident energies of 0.5 and 5.55 MeV are plotted in Fig. 5b. The results from TALYS(GEF) are in better agreement with the experimental data from Ref. [59] at both 0.5 and 5.55 MeV, compared to the thermal data. This could probably be due to the important role these fission data play in fine-tuning the GEF excitation energy sharing. The energy-sorting mechanism in GEF [37] is responsible for the higher average neutron multiplicity from the heavy fragments. As measured by Müller et al. [59], the added excitation energy is mainly shared among the heavy fragments, leading to an increase in $\bar{\nu}_n(A)$ from the heavy fragments. Since TALYS(GEF) uses the excitation energies of GEF directly, it reproduces this effect where a significant increase in $\bar{\nu}_n(A)$ is observed for the heavy fragment mass region. In contrast, the results obtained from TALYS(HF^{3}D) do not exhibit this observed trend. This discrepancy is attributed to the fact that the energy-sorting in the HF^{3}D model is adjusted to reproduce the energy dependence of $\bar{\nu}_n$ [22,23]. TALYS reflects the difference in the energy-sorting mechanism from GEF and HF^{3}D model.

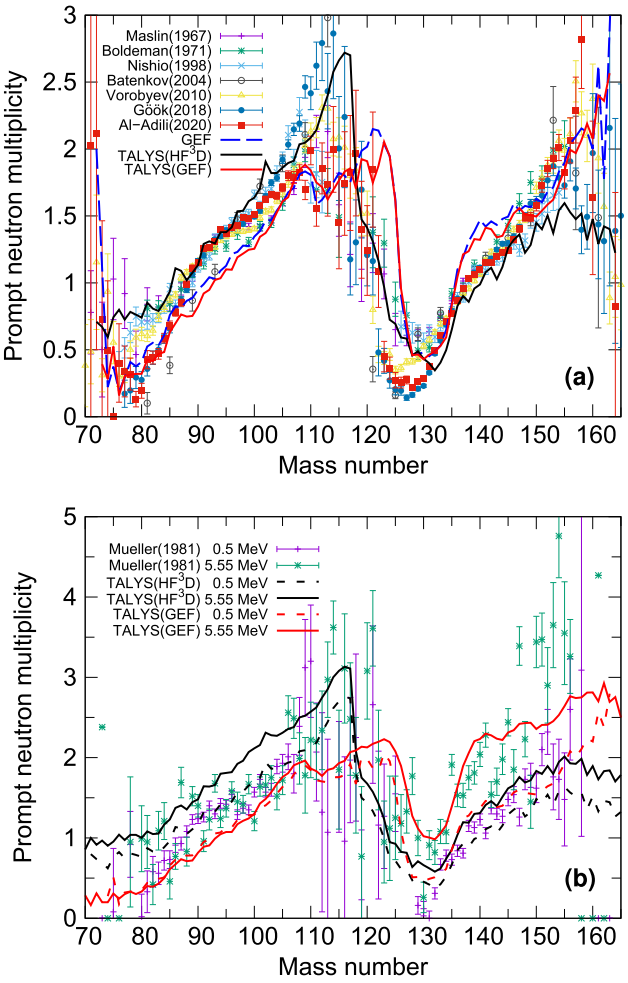

Fig. 5 Mass-dependent neutron multiplicity $\bar{\nu}_n(A)$ in the ^{235}U(n,f) reaction **a** at thermal energy and **b** at the incident energies of 0.5 and 5.55 MeV [59]

Figure 6 represents the $\bar{\nu}_n$ as a function of incident neutron energy ranging from thermal up to 5 MeV. The calculations show an enhanced number of emitted neutrons as a function of incident energy, which is consistent with known data. TALYS(HF^{3}D) successfully reproduces the evaluated value at thermal energy. On the other hand, TALYS(GEF) underestimates the evaluated data at thermal energy by about 0.1, but it agrees with the data as the incident energy increases.

The calculated PFNS$_{(\mathrm{LAB})}$ as ratio to a Maxwellian spectrum at $T_M = 1.32$ MeV is shown in Fig. 7. Both PFNS$_{(\mathrm{LAB})}$ results of TALYS(GEF) and TALYS(HF^{3}D) do not describe the shape of experimental data above 2 MeV outgoing energy, TALYS(HF^{3}D) has a harder tail and TALYS(GEF) has a softer tail of PFNS$_{(\mathrm{LAB})}$. Moreover, the results differ much between TALYS(GEF) and GEF, which reflects the difference in the evaporation scheme in these codes.

4.2.2 *Prompt γ-ray observables*

The experimental data on the number of emitted γ-rays, $\bar{\nu}_\gamma(A)$, is unfortunately still scarce. In recent years, however, the accuracy of the $\bar{\nu}_\gamma$ measurements has improved due to the development in instrumentation and novel detector systems [60]. As a consequence, recent investigations [64] shed more light on the saw-tooth shape in $\bar{\nu}_\gamma(A)$.

The mass-dependent γ-ray multiplicity, $\bar{\nu}_\gamma(A)$, calculated in this work, shows some significant differences between TALYS(GEF) and GEF as seen in Fig. 8a. While GEF has a flatter $\bar{\nu}_\gamma$ as a function of the fragment mass, TALYS results exhibit a more pronounced saw-tooth shape. The results agree fairly well with the experimental data, albeit smaller γ-ray multiplicities are observed around fragment mass numbers $A = 100$ to 110. Other contemporary fission codes, such as FIFRELIN [65], PbP, and DSE [66], also verify the saw-tooth shape in several fissioning systems.

Another important fission observable is the evolution of the total number of released γ-rays as a function of the incident neutron energy, which can be seen in Fig. 8b. A higher excitation energy leads to an increased $\bar{\nu}_\gamma$ similar to the trend observed in the prompt fission neutrons. TALYS agrees generally with GEF and with the evaluated data files. The current evaluation data indicate higher $\bar{\nu}_\gamma$ as it is based on the current experimental and theoretical underlying data. Taking into account these factors, TALYS tends to underestimate the $\bar{\nu}_\gamma$. This underestimation is not fully understood yet but could arise from a non-optimal spin cut-off parameter, which is known to strongly influence the number of emitted γ-rays. Another possible explanation is that older experimental data pointed to a lower total number of emitted γ-rays, which is around 6.5 γ-rays/fission as can be seen in Table 3. In contrast, this value has been increasing as a function of time, where recent experimental studies indicated a number as high as 8.2 γ-rays/fission. The older data might still be used in fine-tuning of excitation energies and spin distributions, which could affect the current calculations.

Another aspect is the energy spectrum of the γ-rays. Figure 9 shows calculated PFGS multiplied by $\bar{\nu}_\gamma$ compared with experimental and evaluated data. A pronounced peak is observed around 0.2 MeV in both TALYS(HF^{3}D) and TALYS(GEF) results. This peak is due to the treatment of bins in the TALYS as mentioned in Sect. 4.1.2. As a consequence, the average energy of emitted γ-rays tends to be lower for TALYS results compared to other data, as shown in Table 3.

4.2.3 *Independent fission product yields*

Figure 10 shows the calculated independent fission product yield as a function of mass $Y(A)$ for ^{235}U(n$_{\mathrm{th}}$,f). The results show an agreement between TALYS(GEF) and stand-alone

Table 3 Multiplicities of prompt neutrons and γ-rays, $\bar{\nu}_n$ and $\bar{\nu}_\gamma$, and the average energies of neutrons and γ-rays, $\langle\epsilon_n\rangle$ and $\langle\epsilon_\gamma\rangle$ for the ^{235}U(n$_{th}$,f) reaction. $\langle\epsilon_n\rangle$ is given in the laboratory frame (LAB), while $\langle\epsilon_\gamma\rangle$ is given in the center-of-mass system (CMS)

	$\bar{\nu}_\gamma$	$\bar{\nu}_n$	$\langle\epsilon_\gamma\rangle$(MeV)	$\langle\epsilon_n\rangle$(MeV)
TALYS(GEF)	6.13	2.30	0.761	1.991
TALYS(HF^{3}D)	6.05	2.41	0.772	2.079
GEF	6.61	2.42	0.962	1.997
Oberstedt et al. [60]	8.19 ± 0.11		0.85 ± 0.02	
Verbinski et al. [61]	6.70 ± 0.30		0.97 ± 0.05	
Pleasonton et al. [62]	6.51 ± 0.30		0.99 ± 0.07	
Peelle et al. [63]	7.45 ± 0.35		0.96 ± 0.05	
ENDF-B/VIII.0	8.58	2.41	0.85	2.00
JEFF-3.3	8.74	2.41	0.81	

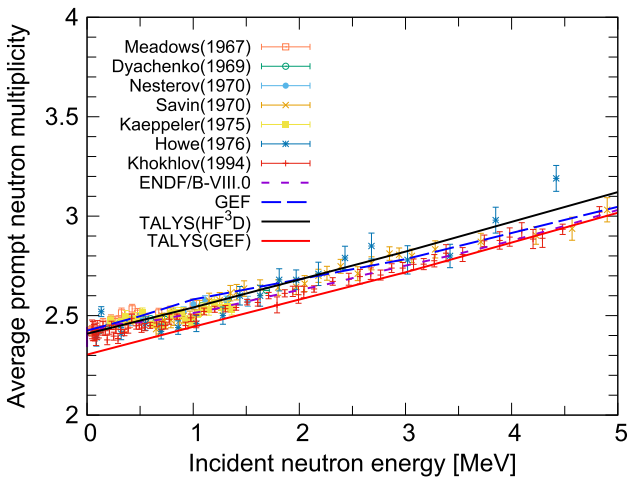

Fig. 6 $\bar{\nu}_n$ as a function of incident energy in the ^{235}U(n,f) reaction

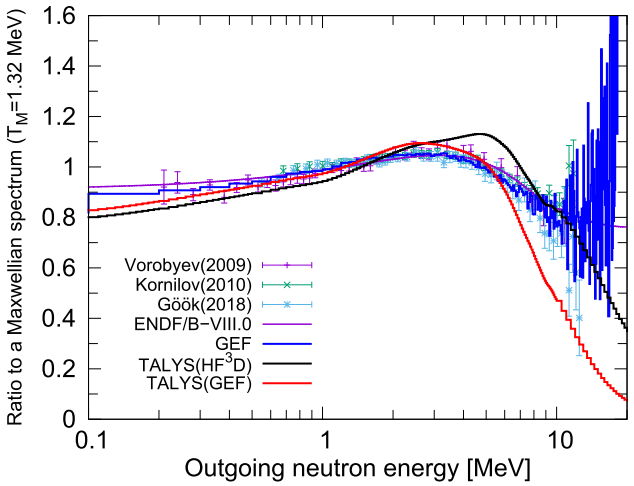

Fig. 7 PFNS$_{(LAB)}$ as ratio to a Maxwellian spectrum at $T_M = 1.32$ MeV in the ^{235}U(n$_{th}$,f) reaction

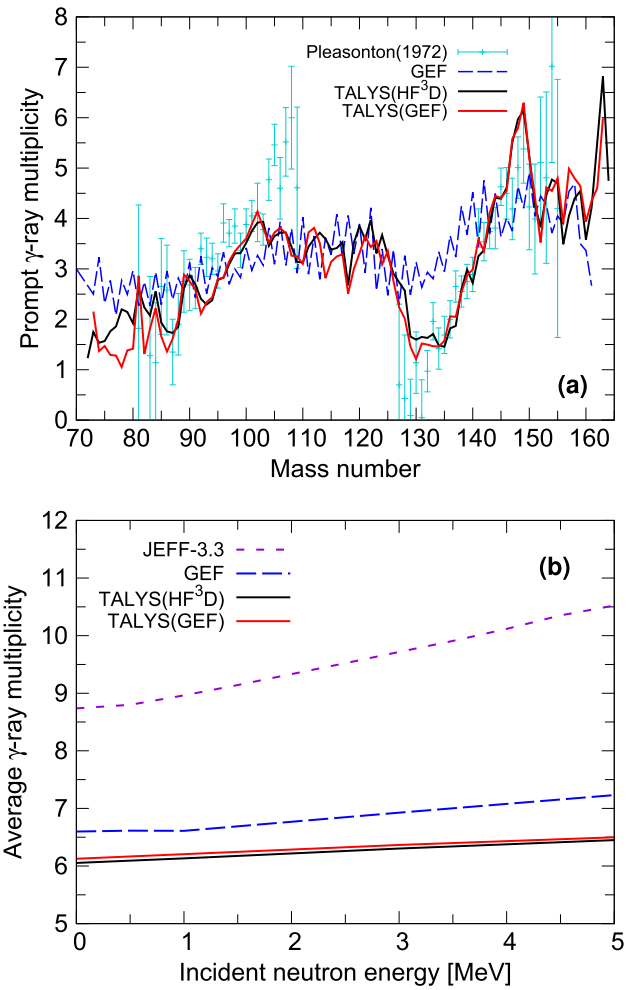

Fig. 8 **a** $\bar{\nu}_\gamma(A)$ for thermal neutron-induced fission on ^{235}U and **b** $\bar{\nu}_\gamma$ as a function of incident energy for neutron-induced fission on ^{235}U

GEF, which could result in a similar treatment in both TALYS and stand-alone GEF on neutron emissions that is strongly related to the neutron separation energy. Both results reproduce the prominent peaks in the fission product yields, for instance around $A = 138$ for heavy fragments and around $A = 94, 100$ for light ones. The peak at $A = 134$ is reproduced in TALYS(GEF), however, TALYS(HF^{3}D) does not

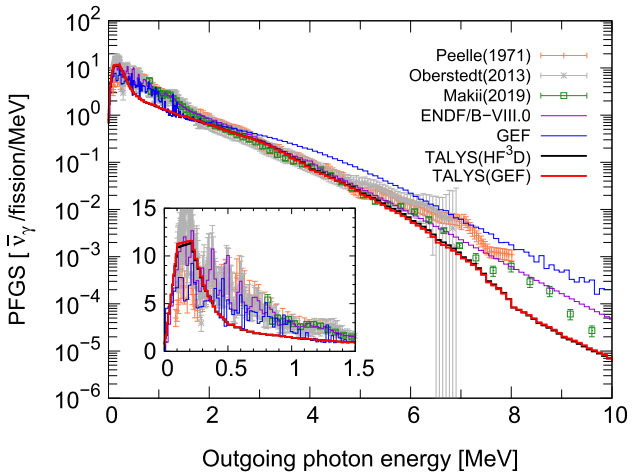

Fig. 9 PFGS multiplied by $\bar{\nu}_\gamma$ in the ^{235}U(n$_{th}$,f) reaction and the inset is its enlarged figure below 1.5 MeV

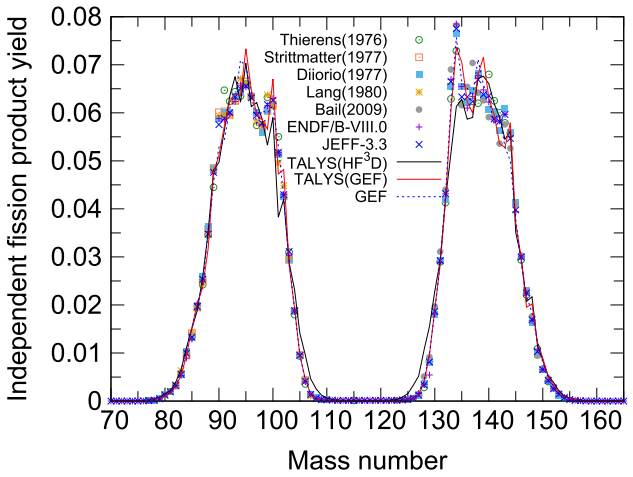

Fig. 10 Independent fission product yields in ^{235}U(n$_{th}$,f)

reproduce the peak while the original HF^{3}D model reproduces [22].

The calculated $Y(Z, A)$ for several fission products were compared with the experimental data from Rudstam et al. [67], as shown in Fig. 11. Both the TALYS(GEF) and TALYS(HF^{3}D) results align well with the experimental data, with the calculated/experimental (C/E) ratio approaching 1.0 for yields above 0.001. However, there is greater dispersion in the C/E for $Y(Z, A)$ below approximately 0.001. Both TALYS results, TALYS(GEF) and TALYS(HF^{3}D), are roughly consistent with the tendency shown in the experimental data where experimental uncertainties are also large.

5 Conclusion

A new approach for calculating nuclear fission data is proposed. This procedure consists of the use of fission codes to provide input for the Hauser-Feshbach formalism of TALYS.

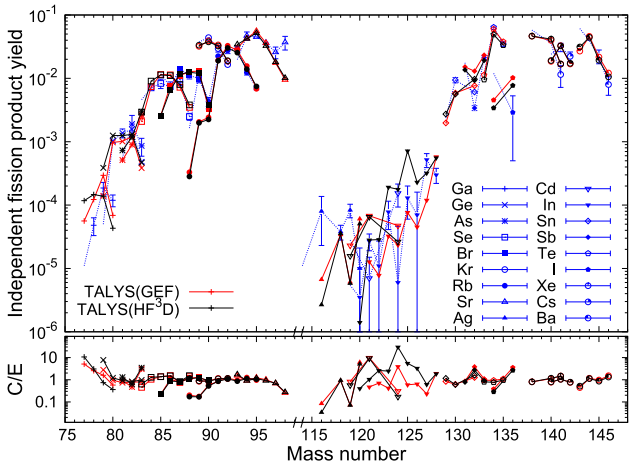

Fig. 11 Comparison of the calculated independent fission product yield $Y(Z, A)$ with the experimental data reported by Rudstam et al. [67] in ^{235}U(n,f) at thermal energy

To illustrate this method, two fission codes, GEF and HF^{3}D, were utilized to create databases that were subsequently used as input for TALYS. The TALYS results are compared with both experimental/evaluated data and the results of the standalone GEF code. The development of such a database has streamlined the inclusion of fission data from other code developers due to the implementation of a standardized format that contains information on fission fragment yields and their excitation energy distributions. The adoption of this new standard format encourages fission model developers to prepare and supply TALYS with input data.

The neutron-induced fission of ^{235}U at incident energies from thermal up to 5 MeV was chosen for the validation of this procedure. We investigated the sensitivity of fission observables on mainly three parameters, namely the number of continuum states (N), the scaling factor for the spin cut-off parameter in the level density formula (f_s), and the scaling factor for the primary fission fragment angular momentum population (f^2). We chose $f^2 = 4$ and $f_s = 0.4$ because they showed a good agreement with neutron observables. Moreover, we selected $N = 300$ particularly fine-tuned for the average total γ-ray multiplicity.

During the investigation, TALYS showed a decent agreement with the experimental data of prompt neutron observables, e.g., the saw-tooth shapes of $\bar{\nu}_n(A)$ and the total average number of prompt neutrons as a function of incident energy. Significant differences were however observed between TALYS(GEF) and TALYS(HF^{3}D) results, highlighting again the importance of different physical considerations and assumptions on the energy partition in fission. The prompt neutron spectrum results of both TALYS(GEF) and TALYS(HF^{3}D) do not describe the shape exhibited by the experimental data, pointing to the need for further investigations and model adjustments.

Regarding the prompt γ-ray observables, the TALYS results tend to show a saw-tooth shape of $\bar{\nu}_\gamma(A)$, which agrees with recent experimental findings. Despite this, the $\bar{\nu}_\gamma$ is underestimated in absolute scale. The total prompt fission γ-ray spectrum (PFGS) exhibits a strong peak around 0.2 MeV, which is believed to be a binning effect in the TALYS code, and it underestimates the experimental data in some regions e.g., below 2 MeV and after 6 MeV.

The independent fission product yield $Y(A)$ of TALYS(GEF) is in overall good agreement with the experimental data and the recent evaluations, reproducing the pronounced peaks (at $A = 134, 138, 100, 94$) and dips in the independent fission product yield structure. For $Y(Z, A)$, both TALYS results are generally consistent with the literature data.

In the future, more correlated physical quantities will be studied, such as cumulative fission product yield, γ-ray observables, and isomeric yield ratios. TALYS has been earlier employed, to calculate isomeric yield ratios based on different assumed angular momentum generation in the nascent fission fragments [68–71]. However, these calculations focus on individual isomeric yield ratios and utilize an external spin-energy matrix implementation. Moreover, no particular emphasis was put on the other fission observables. The outlook from this work is to exploit the new implementation of internal looping to generate systematic global isomeric yield ratio investigations as a function of mass and excitation energy taking into account the correlation between different fission observables.

Acknowledgements The authors thank T. Kawano (Los Alamos National Laboratory) and K.-H. Schmidt for valuable discussions. The IAEA-NDS acknowledges the internship program "The Nuclear Regulation Human Resource Development Program (ANSET: Advanced Nuclear 3 S Education and Training)" entrusted to Tokyo Institute of Technology, Tokyo, Japan by the Nuclear Regulation Agency of Japan, for supporting this work. A. A. would like to acknowledge Liljewalch travel scholarships and Ingegerd Berghs stiftelse for their research grants.

Data Availability Statement This manuscript has no associated data or the data will not be deposited. [Authors' comment: The datasets generated and/or analyzed during the current study are available and reproducible in/by the open-source nuclear reaction model code, TALYS.]

References

1. P. Dimitriou, I. Dillmann, B. Singh, V. Piksaikin, K.P. Rykaczewski, J.L. Tain, A. Algora, K. Banerjee, I.N. Borzov, D. Cano-Ott, S. Chiba, M. Fallot, D. Foligno, R. Grzywacz, X. Huang, T. Marketin, F. Minato, G. Mukherjee, B.C. Rasco, A. Sonzogni, M. Verpelli, A. Egorov, M. Estienne, L. Giot, D. Gremyachkin, M. Madurga, E.A. McCutchan, E. Mendoza, K.V. Mitrofanov, M. Narbonne, P. Romojaro, A. Sanchez-Caballero, N.D. Scielzo. Development of a reference database for beta-delayed neutron emission. Nucl. Data Sheets, **173**, 144–238 (2021) **(Special Issue on Nuclear Reaction Data)**
2. Fission Product Yield Data for the Transmutation of Minor Actinide Nuclear Waste. Number STI/PUB/1286 in non-serial publications. International Atomic Energy Agency, Vienna (2008)
3. Karolina Kolos, Vladimir Sobes, Ramona Vogt, Catherine E. Romano, Michael S. Smith, Lee A. Bernstein, David A. Brown, Mary T. Burkey, Yaron Danon, Mohamed A. Elsawi, Bethany L. Goldblum, Lawrence H. Heilbronn, Susan L. Hogle, Jesson Hutchinson, Ben Loer, Elizabeth A. McCutchan, Matthew R. Mumpower, Ellen M. O'Brien, Catherine Percher, Patrick N. Peplowski, Jennifer J. Ressler, Nicolas Schunck, Nicholas W. Thompson, Andrew S. Voyles, William Wieselquist, Michael Zerkle, Current nuclear data needs for applications. Phys. Rev. Res. **4**, 021001 (2022)
4. T. R. England , B.F. Rider. Evaluation and compilation of fission product yields. Technical Report ENDF-349, LA-UR-94-3106, Los Alamos National Laboratory (1994)
5. A.C. Wahl, Nuclear-charge distribution and delayed-neutron yields for thermal-neutron-induced fission of ^{235}U, ^{233}U, and ^{239}Pu and for spontaneous fission of ^{252}Cf. At. Data Nucl. Data Tables **39**(1), 1–156 (1988)
6. A. C. Wahl, Systematics of fission-product yields. Technical Report LA-13928, Los Alamos National Laboratory (2002)
7. D.G. Madland, T.R. England, The influence of isomeric states on independent fission product yields. Nucl. Sci. Eng. **64**, 859–865 (1977)
8. D. A. Brown, M. B. Chadwick, R. Capote, A. C. Kahler, A. Trkov, M. W. Herman, A. A. Sonzogni, Y. Danon, A. D. Carlson, M. Dunn, D. L. Smith, G. M. Hale, G. Arbanas, R. Arcilla, C. R. Bates, B. Beck, B. Becker, F. Brown, R. J. Casperson, J. Conlin, D. E. Cullen, M. A. Descalle, R. Firestone, T. Gaines, K. H. Guber, A. I. Hawari, J. Holmes, T. D. Johnson, T. Kawano, B. C. Kiedrowski, A. J. Koning, S. Kopecky, L. Leal, J. P. Lestone, C. Lubitz, J. I. Márquez Damián, C. M. Mattoon, E. A. McCutchan, S. Mughabghab, P. Navratil, D. Neudecker, G. P. A. Nobre, G. Noguere, M. Paris, M. T. Pigni, A. J. Plompen, B. Pritychenko, V. G. Pronyaev, D. Roubtsov, D. Rochman, P. Romano, P. Schillebeeckx, S. Simakov, M. Sin, I. Sirakov, B. Sleaford, V. Sobes, E. S. Soukhovitskii, I. Stetcu, P. Talou, I. Thompson, S. van der Marck, L. Welser-Sherrill, D. Wiarda, M. White, J. L. Wormald, R. Q. Wright, M. Zerkle, G. Žerovnik, Y. Zhu. ENDF/B-VIII.0: the 8th major release of the nuclear reaction data library with CIELO-project cross sections, new standards and thermal scattering data. Nucl. Data Sheets **148**, 1–142 (2018)
9. K. Shibata, O. Iwamoto, T. Nakagawa, N. Iwamoto, A. Ichihara, S. Kunieda, S. Chiba, K. Furutaka, N. Otuka, T. Ohsawa, T. Murata, H. Matsunobu, A. Zukeran, S. Kamada, J. Katakura, JENDL-4.0: a new library for nuclear science and engineering. J. Nucl. Sci. Technol. **48**, 1–30 (2011)
10. David G. Madland, J. Rayford Nix, New calculation of prompt fission neutron spectra and average prompt neutron multiplicities. Nucl. Sci. Eng. **81**(2), 213–271 (1982)

11. Patrick Jaffke, Identifying inconsistencies in fission product yield evaluations with prompt neutron emission. Nucl. Sci. Eng. **190**(3), 258–270 (2018)
12. P. Talou, B. Becker, T. Kawano, M.B. Chadwick, Y. Danon, Advanced monte carlo modeling of prompt fission neutrons for thermal and fast neutron-induced fission reactions on ^{239}Pu. Phys. Rev. C **83**, 064612 (2011)
13. K.A.W.A.N.O. Toshihiko, T.A.L.O.U. Patrick, B.C.H.A.D. W.I.C.K. Mark, W.A.T.A.N.A.B.E. Takehito, monte carlo simulation for particle and -ray emissions in statistical Hauser–Feshbach model. J. Nucl. Sci. Technol. **47**(5), 462–469 (2010)
14. Jørgen. Randrup, Ramona Vogt, Calculation of fission observables through event-by-event simulation. Phys. Rev. C **80**, 024601 (2009)
15. R. Vogt, J. Randrup, J. Pruet, W. Younes, Event-by-event study of prompt neutrons from ^{239}Pu(n, f). Phys. Rev. C **80**, 044611 (2009)
16. O. Litaize, O. Serot, Investigation of phenomenological models for the Monte Carlo simulation of the prompt fission neutron and γ emission. Phys. Rev. C **82**, 054616 (2010)
17. S. Lemaire, P. Talou, T. Kawano, M.B. Chadwick, D.G. Madland, Monte Carlo approach to sequential neutron emission from fission fragments. Phys. Rev. C **72**, 024601 (2005)
18. S. Lemaire, P. Talou, T. Kawano, M.B. Chadwick, D.G. Madland, Monte Carlo approach to sequential γ-ray emission from fission fragments. Phys. Rev. C **73**, 014602 (2006)
19. K.-H. Schmidt, B. Jurado, C. Amouroux, C. Schmitt, General description of fission observables: GEF model code. Nucl. Data Sheets **131**, 107–221 (2016). (**Special Issue on Nuclear Reaction Data**)
20. A. Tudora, F.J. Hambsch, Comprehensive overview of the Point-by-Point model of prompt emission in fission. Eur. Phys. J. A **53**(8), 159 (2017)
21. Anabella Tudora, Influence of energy partition in fission and pre-neutron fragment distributions on post-neutron fragment yields, application for 235u(nth, f). Eur. Phys. J. A **58**(7), 126 (2022)
22. S. Okumura, T. Kawano, P. Jaffke, P. Talou, S. Chiba, ^{235}U(n, f) independent fission product yield and isomeric ratio calculated with the statistical Hauser-Feshbach theory. J. Nucl. Sci. Technol. **55**(9), 1009–1023 (2018)
23. Shin Okumura, Toshihiko Kawano, Amy Elizabeth Lovell, Tadashi Yoshida, Energy dependent calculations of fission product, prompt, and delayed neutron yields for neutron induced fission on 235u, 238u, and 239pu. J. Nucl. Sci. Technol. **59**(1), 96–109 (2022)
24. A.E. Lovell, T. Kawano, S. Okumura, I. Stetcu, M.R. Mumpower, P. Talou, Extension of the Hauser-Feshbach fission fragment decay model to multichance fission. Phys. Rev. C **103**, 014615 (2021)
25. J.-F. Lemaître, S. Goriely, S. Hilaire, J.-L. Sida, Fully microscopic scission-point model to predict fission fragment observables. Phys. Rev. C **99**, 034612 (2019)
26. A.J. Koning, D. Rochman, Modern nuclear data evaluation with the TALYS code system. Nucl. Data Sheets **113**(12), 2841–2934 (2012). (**Special Issue on Nuclear Reaction Data**)
27. Ulrich Brosa, Siegfried Grossmann, Andreas Muller, Nuclear scission. Phys. Rep. **197**(4), 167–262 (1990)
28. M.C. Duijvestijn, A.J. Koning, F.-J. Hambsch, Mass distributions in nucleon-induced fission at intermediate energies. Phys. Rev. C **64**, 014607 (2001)
29. A. Al-Adili. Measurements of the ^{234}U(n,f) reaction with a Frisch-Grid Ionization Chamber up to $E_n = 5$ MeV. PhD thesis, Uppsala University (2013)
30. F. Nordström. Benchmark of the fission channels in TALYS. Technical Report UPTEC ES 21016, Uppsala University (2021)
31. K. Fujio, S. Okumura, A. Koning, New development in TALYS—fission fragment statistical decay model. In: Proceedings of the 2021 Symposium on Nuclear Data; November 18–19, 2021, Online Connection Conference, (JAEA-Conf 2022-001) (2021)
32. K. Fujio, S. Okumura, A. Koning. Fission fragment decay calculation by the Hauser-Feshbach statistical decay theory in TALYS 1.96. Technical Report IAEA(NDS)-0239, International Atomic Energy Agency (2022)
33. S. Goriely, N. Chamel, J. M. Pearson Hartree-fock-bogoliubov nuclear mass model with 0.50 mev accuracy based on standard forms of skyrme and pairing functionals. Phys. Rev. C **88**, 061302 (2013)
34. P. Helgesson, H. Sjostrand, Treating model defects by fitting smoothly varying model parameters: energy dependence in nuclear data evaluation. Ann. Nucl. Energy **120**, 35–47 (2018)
35. G. Schnabel, H. Sjostrand, J. Hansson, D. Rochman, A. Koning, R. Capote, Conception and software implementation of a nuclear data evaluation pipeline. Nucl. Data Sheets **173**, 239–284 (2021). (**Special Issue on Nuclear Reaction Data**)
36. T. Ohsawa, T. Horiguchi, M. Mitsuhashi, Multimodal analysis of prompt neutron spectra for ^{238}Pu(sf), ^{240}Pu(sf), ^{242}Pu(sf) and ^{239}Pu(n_{th}, f). Nucl. Phys. A **665**(1), 3–12 (2000)
37. Karl-Heinz. Schmidt, Beatriz Jurado, Entropy driven excitation energy sorting in superfluid fission dynamics. Phys. Rev. Lett. **104**, 212501 (2010)
38. I. Stetcu, A.E. Lovell, P. Talou, T. Kawano, S. Marin, S.A. Pozzi, A. Bulgac, Angular momentum removal by neutron and γ-ray emissions during fission fragment decays. Phys. Rev. Lett. **127**, 222502 (2021)
39. J.N. Wilson, D. Thisse, M. Lebois, N. Jovančević, D. Gjestvang, R. Canavan, M. Rudigier, D. Étasse, R.-B. Gerst, L. Gaudefroy, E. Adamska, P. Adsley, A. Algora, M. Babo, K. Belvedere, J. Benito, G. Benzoni, A. Blazhev, A. Boso, S. Bottoni, M. Bunce, R. Chakma, N. Cieplicka-Oryńczak, S. Courtin, M.L. Cortés, P. Davies, C. Delafosse, M. Fallot, B. Fornal, L. Fraile, A. Gottardo, V. Guadilla, G. Häfner, K. Hauschild, M. Heine, C. Henrich, I. Homm, F. Ibrahim, ŁW. Iskra, P. Ivanov, S. Jazrawi, A. Korgul, P. Koseoglou, T. Kröll, T. Kurtukian-Nieto, L. Le Meur, S. Leoni, J. Ljungvall, A. Lopez-Martens, R. Lozeva, I. Matea, K. Miernik, J. Nemer, S. Oberstedt, W. Paulsen, M. Piersa, Y. Popovitch, C. Porzio, L. Qi, D. Ralet, P.H. Regan, K. Rezynkina, V. Sánchez-Tembleque, S. Siem, C. Schmitt, P.-A. Söderström, C. Sürder, G. Tocabens, V. Vedia, D. Verney, N. Warr, B. Wasilewska, J. Wiederhold, M. Yavahchova, F. Zeiser, S. Ziliani, Angular momentum generation in nuclear fission. Nature **590**(7847), 566–570 (2021)
40. Aurel Bulgac, Ibrahim Abdurrahman, Shi Jin, Kyle Godbey, Nicolas Schunck, Ionel Stetcu, Fission fragment intrinsic spins and their correlations. Phys. Rev. Lett. **126**, 142502 (2021)
41. Petar Marević, Nicolas Schunck, Jørgen. Randrup, Ramona Vogt, Angular momentum of fission fragments from microscopic theory. Phys. Rev. C **104**, L021601 (2021)
42. Aurel Bulgac, Ibrahim Abdurrahman, Kyle Godbey, Ionel Stetcu, Fragment intrinsic spins and fragments' relative orbital angular momentum in nuclear fission. Phys. Rev. Lett. **128**, 022501 (2022)
43. H.A. Bethe, An attempt to calculate the number of energy levels of a heavy nucleus. Phys. Rev. **50**, 332–341 (1936)
44. S. Goriely, A new nuclear level density formula including shell and pairing correction in the light of a microscopic model calculation. Nucl. Phys. A **605**(1), 28–60 (1996)
45. S.F. Mughabghab, C. Dunford, Nuclear level density and the effective nucleon mass. Phys. Rev. Lett. **81**, 4083–4086 (1998)
46. A.J. Koning, J.P. Delaroche, Local and global nucleon optical models from 1 kev to 200 mev. Nucl. Phys. A **713**(3), 231–310 (2003)
47. A. Gilbert, A.G.W. Cameron, A composite nuclear-level density formula with shell corrections. Can. J. Phys. **43**, 1446–1496 (1965)
48. A.J. Koning, S. Hilaire, S. Goriely, Global and local level density models. Nucl. Phys. A **810**(1), 13–76 (2008)
49. S. Goriely, P. Dimitriou, M. Wiedeking, T. Belgya, R. Firestone, J. Kopecky, M. Krticka, V. Plujko, R. Schwengner, S. Siem, H. Utsunomiya, S. Hilaire, S. Peru, Y.S. Cho, D.M. Filipescu, N.

Iwamoto, T. Kawano, V. Varlamov, R. Xu, Reference database for photon strength functions. Eur. Phys. J. A **55**(10), 172 (2019)
50. V.A. Plujko, O.M. Gorbachenko, R. Capote, P. Dimitriou, Giant dipole resonance parameters of ground-state photoabsorption: experimental values with uncertainties. At. Data Nucl. Data Tables **123–124**, 1–85 (2018)
51. S. Goriely, V. Plujko, Simple empirical $e1$ and $m1$ strength functions for practical applications. Phys. Rev. C **99**, 014303 (2019)
52. R. Capote, M. Herman, P. Obložinský, P.G. Young, S. Goriely, T. Belgya, A.V. Ignatyuk, A.J. Koning, S. Hilaire, V.A. Plujko, M. Avrigeanu, O. Bersillon, M.B. Chadwick, T. Fukahori, Z. Ge, Y. Han, S. Kailas, J. Kopecky, V.M. Maslov, G. Reffo, M. Sin, ESh. Soukhovitskii, P. Talou, RIPL—reference input parameter library for calculation of nuclear reactions and nuclear data evaluations. Nucl. Data Sheets **110**(12), 3107–3214 (2009)
53. N. Feather. Emission of neutrons from moving fission fragments. Technical Report BM-148, British Mission (1942)
54. James Terrell, Fission neutron spectra and nuclear temperatures. Phys. Rev. **113**, 527–541 (1959)
55. D.G. Madland, A.C. Kahler, Refinements in the los alamos model of the prompt fission neutron spectrum. Nucl. Phys. A **957**, 289–311 (2017)
56. A. Rodrigo, N. Otuka, S. Takács, A. J. Koning, Compilation of isomeric ratios of light particle induced nuclear reactions (2023). arXiv:2303.09595
57. A. J. M. Plompen, O. Cabellos, C. De Saint Jean, M. Fleming, A. Algora, M. Angelone, P. Archier, E. Bauge, O. Bersillon, A. Blokhin, F. Cantargi, A. Chebboubi, C. Diez, H. Duarte, E. Dupont, J. Dyrda, B. Erasmus, L. Fiorito, U. Fischer, D. Flammini, D. Foligno, M. R. Gilbert, J. R. Granada, W. Haeck, F. J. Hambsch, P. Helgesson, S. Hilaire, I. Hill, M. Hursin, R. Ichou, R. Jacqmin, B. Jansky, C. Jouanne, M. A. Kellett, D. H. Kim, H. I. Kim, I. Kodeli, A. J. Koning, A. Yu. Konobeyev, S. Kopecky, B. Kos, A. Krása, L. C. Leal, N. Leclaire, P. Leconte, Y. O. Lee, H. Leeb, O. Litaize, M. Majerle, J. I. Márquez Damián, F. Michel-Sendis, R. W. Mills, B. Morillon, G. Noguère, M. Pecchia, S. Pelloni, P. Pereslavtsev, R. J. Perry, D. Rochman, A. Röhrmoser, P. Romain, P. Romojaro, D. Roubtsov, P. Sauvan, P. Schillebeeckx, K. H. Schmidt, O. Serot, S. Simakov, I. Sirakov, H. Sjöstrand, A. Stankovskiy, J. C. Sublet, P. Tamagno, A. Trkov, S. van der Marck, F. Álvarez-Velarde, R. Villari, T. C. Ware, K. Yokoyama, G. Žerovnik, The joint evaluated fission and fusion nuclear data library, JEFF-3.3. Eur. Phys. J. A, **56**(7), 181 (2020)
58. A. Al-Adili, D. Tarrío, K. Jansson, V. Rakopoulos, A. Solders, S. Pomp, A. Göök, F.-J. Hambsch, S. Oberstedt, M. Vidali, Prompt fission neutron yields in thermal fission of ^{235}U and spontaneous fission of ^{252}Cf. Phys. Rev. C **102**, 064610 (2020)
59. R. Müller, A.A. Naqvi, F. Käppeler, F. Dickmann, Fragment velocities, energies, and masses from fast neutron induced fission of ^{235}U. Phys. Rev. C **29**, 885–905 (1984)
60. A. Oberstedt, T. Belgya, R. Billnert, R. Borcea, T. Bryś, W. Geerts, A. Göök, F.-J. Hambsch, Z. Kis, T. Martinez, S. Oberstedt, L. Szentmiklosi, K. Takàcs, M. Vidali, Improved values for the characteristics of prompt-fission γ-ray spectra from the reaction ^{235}u$(n_{\rm th}, f)$. Phys. Rev. C **87**, 051602 (2013)
61. V.V. Verbinski, H. Weber, R.E. Sund, Prompt gamma rays from ^{235}U(n, f), ^{239}Pu(n, f), and spontaneous fission of ^{252}Cf. Phys. Rev. C **7**, 1173–1185 (1973)
62. Frances Pleasonton, Robert L. Ferguson, H.W. Schmitt, Prompt gamma rays emitted in the thermal-neutron-induced fission of ^{235}U. Phys. Rev. C **6**, 1023–1039 (1972)
63. R.W. Peelle, F.C. Maienschein, Spectrum of photons emitted in coincidence with fission of ^{235}U by thermal neutrons. Phys. Rev. C **3**, 373–390 (1971)
64. M. Travar, V. Piau, A. Gook, O. Litaize, J. Nikolov, A. Oberstedt, S. Oberstedt, J. Enders, M. Peck, W. Geerts, M. Vidali, Experimental information on mass- and tke-dependence of the prompt fission -ray multiplicity. Phys. Lett. B **817**, 136293 (2021)
65. O. Litaize, O. Serot, L. Berge, Fission modelling with FIFRELIN. Eur. Phys. J. A **51**(12), 177 (2015)
66. Anabella Tudora, Prompt γ-ray results of two deterministic modelings of prompt emission in fission. Eur. Phys. J. A **56**(5), 128 (2020)
67. G. Rudstam, P. Aagaard, B. Ekström, E. Lund, H. Göktürk, H.U. Zwicky, Yields of products from thermal neutron-induced fission of ^{235}u. Radiochim. Acta **49**(4), 155–192 (1990)
68. A. Al-Adili, V. Rakopoulos, A. Solders, Extraction of angular momenta from isomeric yield ratios—employing talys to de-excite primary fission fragments. Eur. Phys. J. A **55**(4), 61 (2019)
69. A. Al-Adili, A. Solders, V. Rakopoulos, Employing talys to deduce angular momentum root mean-square values, Jrms, in fission fragments. EPJ Web Conf. **239**, 03019 (2020)
70. V. Rakopoulos, M. Lantz, A. Solders, A. Al-Adili, A. Mattera, L. Canete, T. Eronen, D. Gorelov, A. Jokinen, A. Kankainen, V.S. Kolhinen, I.D. Moore, D.A. Nesterenko, H. Penttilä, I. Pohjalainen, S. Rinta-Antila, V. Simutkin, M. Vilén, A. Voss, S. Pomp, First isomeric yield ratio measurements by direct ion counting and implications for the angular momentum of the primary fission fragments. Phys. Rev. C **98**, 024612 (2018)
71. V. Rakopoulos, M. Lantz, S. Pomp, A. Solders, A. Al-Adili, L. Canete, T. Eronen, A. Jokinen, A. Kankainen, A. Mattera, I.D. Moore, D.A. Nesterenko, M. Reponen, S. Rinta-Antila, A. de Roubin, M. Vilén, M. Österlund, H. Penttilä, Isomeric fission yield ratios for odd-mass cd and in isotopes using the phase-imaging ion-cyclotron-resonance technique. Phys. Rev. C **99**, 014617 (2019)